ISSN 0021-3640, JETP Letters, 2011, Vol. 93, No. 12, pp. 720–724. © Pleiades Publishing, Inc., 2011.
Original Russian Text © M.R. Shcherbakov, B.B. Tsema, A.A. Ezhov, V.I. Panov, A.A. Fedyanin, 2011, published in Pis'ma v Zhurnal Eksperimental'noi i Teoreticheskoi Fiziki, 2011, Vol. 93, No. 12, pp. 801–806.

Near-Field Optical Polarimetry of Plasmonic Nanowires¶

M. R. Shcherbakov[a], B. B. Tsema[a, b], A. A. Ezhov[a], V. I. Panov[a], and A. A. Fedyanin[a]

[a] *Moscow State University, Faculty of Physics, Moscow, 119991 Russia*

[b] *Moscow State Technical University of Radio Engineering, Electronics, and Automation, pr. Vernadskogo 78, Moscow, 119454 Russia*

e-mail: fedyanin@nanolab.phys.msu.ru

Received June 23, 2011

Local polarization properties of a gold subwavelength grating with plasmon-induced linear dichroism are studied by scanning near-field optical dynamic polarimetry. Periodic modulation of linear dichroism with the period corresponding to the period of the grating and the contrast of 0.3 is found at the distance of $\lambda/20$ from the sample.

DOI: 10.1134/S0021364011120149

The development of nanophotonics as a prospective area of contemporary optics is defined by the growing demand in new solutions in the areas of storage and communication of optical data. One of the disciplines within nanophotonics is nanoplasmonics which is based on various types of plasmon-polaritons comprising coupled oscillations of electromagnetic field and free electrons at the conductor-dielectric interface. Achievements in this field include superfocusing of optical radiation [1], energy transport by plasmonic waveguides and waveguide-based components [2], as well as plasmonic logic elements [3].

Scanning near-field optical microscopy (SNOM) [4] is the method allowing one to study optical properties of plasmon-active media with the direct observation of the local plasmonic field intensity with spatial resolution below the diffraction limit. Ultrafast [5], nonlinear [6] and polarization [7–10] properties of plasmonic nanoobjects have been studied by means of SNOM. In this paper, SNOM is used for the studies of local polarization properties of a subwavelength metallic nanograting under the local plasmon resonance condition. Ordered arrays of gold nanowires (nanogratings) are of interest because of their remarkable polarization properties [11–13].

Nanograting samples were fabricated by electron beam lithography with the lift-off technique on a fused silica substrate with the size of the nanostructured area of 30×30 μm^2. The dimensions of its elements were obtained by atomic force microscopy (AFM) and scanning electronic microscopy. The average width of the nanowires was 80 ± 5 nm, the height is 40 ± 5 nm and the period of the grating is 300 ± 10 nm. Such structure parameters forbid the light diffraction of the illumination used in the experiment and allow the effective excitation of local plasmon-polaritons in an individual wire [11]. The sample series was fabricated with the use of a single template file with a different dose of the electron beam exposure within which the deviation of the sample dimensions is less than 10%. For the SNOM experiments the sample with the highest Q-factor of the plasmon-induced extinction resonance was chosen. An AFM-image of the sample surface is shown in the inset of Fig. 1. The elements of the array are shown to be well-ordered and reproducible.

Far-field transmission spectroscopy, $T(\lambda)$, was performed using a microspectropolarimetry setup allowing one to obtain spectra from small-sized samples [12]. Transmittance spectra were measured for orientations of the incident light polarization parallel and perpendicular to the nanowires. Figure 1 shows the transmittance spectra of a sample with the highest Q-factor of the extinction resonance which manifests itself as a dip in the spectrum. The extinction takes place due to resonant amplification of the electromagnetic field density near the wires illuminated with the light polarized perpendicular to the wires. The resonance quality factor is equal to $Q \simeq 8.3$. Polarizability $p(\omega)$ of the subwavelength particle is proportional to the local field factor [14]:

$$p(\omega) \sim \frac{1}{L[\varepsilon(\omega) - \varepsilon_0] + \varepsilon_0}, \quad (1)$$

where $\varepsilon(\omega)$ is dielectric permittivity of the particle, ε_0 is dielectric permittivity of the surrounding material and L is a coefficient defined by the dimensions of the particle. At the frequency which zeroes the denominator of Eq. (1) an extinction resonance of local plasmon-polaritons occurs due to the increase of the mean electron kinetic energy and its absorption due to electron-lattice interaction. In the nanowires under study $L \cong 0.21$ and the denominator tends to zero at $\lambda \cong$

The article was translated by the authors.

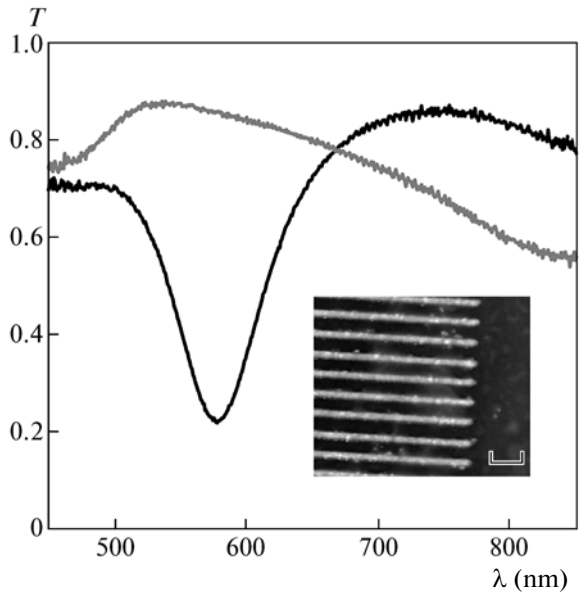

Fig. 1. Transmission spectra of light polarized (gray curve) along and (black curve) perpendicular to the golden nanowires. The dashed line denotes the central wavelength of the laser used in the SNOM experiments. The inset shows the AFM image of the edge of the sample. The scale bar corresponds to 500 nm.

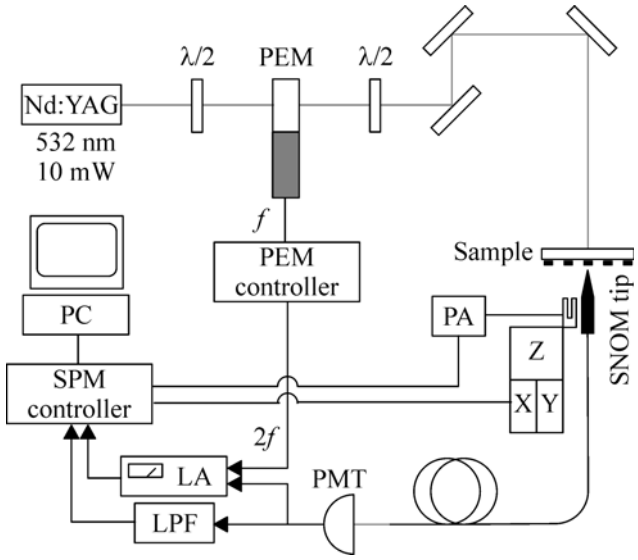

Fig. 2. Schematic of the setup for the plasmonic nanogratings near-field optical microscopy: λ/2 are half-wave plates, PEM is a photoelastic modulator, XYZ is a three-axes piezo-scanner, PA is a tuning fork signal preamplifier, PMT is a photomultiplier tube, LPF is a low-pass filter, and LA is a lock-in amplifier.

580 nm which coincides with the experimentally obtained absorption maximum. There are no remarkable peculiarities in the transmission spectrum of the light polarized parallel to the nanowires. The effect of polarizing light with local plasmons differs significantly from the polarization effect in the wire-grid polarizers which polarize the transmitted radiation perpendicularly to the wires [15].

Transmittance of the linearly polarized light depends on the incident light polarization plane orientation due to linear dichroism effect. Polarization states of the light polarized along or perpendicular to the nanowires are the eigenstates of the structure under study due to symmetry considerations. The linear dichroism value in the far-field is defined as a normalized difference in transmittance measured for polarization eigenstates. The dichroism value reaches 0.6 at the central wavelength of the plasmonic resonance.

Near-field polarization properties of plasmonic nanogratings were investigated by means of scanning near-field dynamic polarimetry setup built on the basis of a scanning probe microscope Solver PRO-M (NT-MDT, Russia) and a photoelastic modulator PEM-100 FS-47/II (Hinds Instruments, USA). The setup is shown schematically in Fig. 2. Horizontally polarized light from a frequency-doubled CW Nd:YAG laser with $\lambda = 532$ nm and power of 10 mW passes through a half-wave plate with its axis oriented at 22.5° with respect to the optical table. Diagonally polarized light passes through the PEM that temporally modulates the phase shift between vertically and horizontally polarized components. The phase shift undergoes harmonic oscillations $\phi(t) = A\sin(2\pi ft)$, where A is the phase shift oscillations amplitude and f is the PEM operating frequency which is equal to 47 kHz. If $A = \pi$, the polarization state output from the PEM changes from diagonal to antidiagonal with the $2f$ frequency.

A half-wave plate placed behind the PEM is used for transformation of the polarization modulation from diagonal/antidiagonal to horizontal/vertical. Mirrors are used to deliver the light onto the sample through the substrate. Optical signal is then collected by an aperture SNOM fiber probe MF002 (NT-MDT, Russia) with the aperture diameter of 50–100 nm. The distance between the probe and the surface is kept constant by a feedback system based on a tuning fork with the preamplifier described in [16]. The distance between the probe and the sample is about λ/20 and controlled by a three-axis piezo-scanner. The collected signal is sent to a photomultiplier tube (PMT) and then divided into two channels. The first channel is connected to a lock-in amplifier which detects the signal modulation amplitude U_{2f} at the $2f$ frequency which is caused by the linear dichroism. The second channel is a low pass filter with the cutoff frequency of 600 Hz. Both signals are then sent to the ADC of the Solver PRO-M controller. Consequently both signals, U_{2f}, which is a measure of the linear dichroism, and

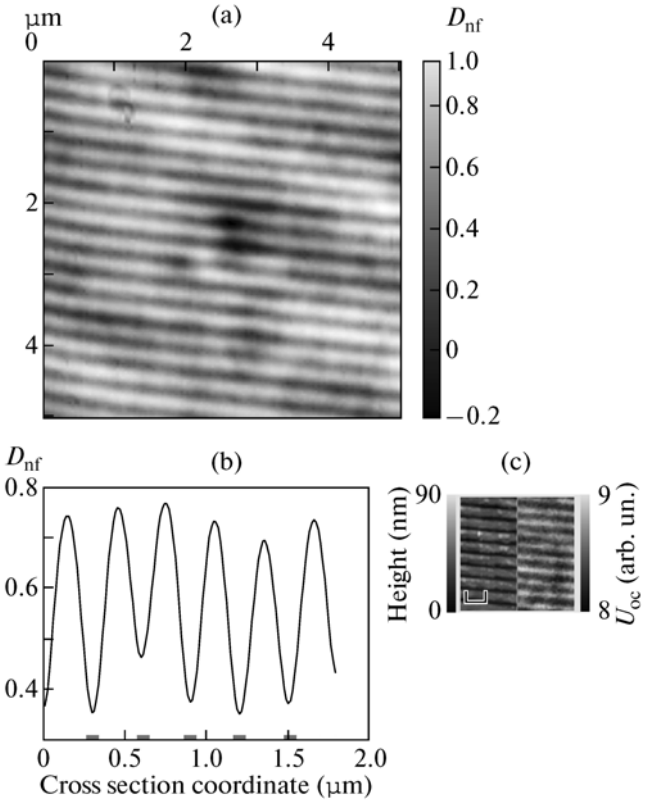

Fig. 3. (a) Spatial distribution of the linear dichroism D_{nf} in the vicinity of the nanograting sample. (b) The cross-section taken along the white line in Fig. 3a. The gray rectangles denote the nanowires position with respect to the linear dichroism map. (c) Superimposed fragments of (right) optical signal and (left) topography images of the same sample area obtained in the two-pass regime. The scale bar corresponds to 500 nm.

U_{DC}, which is proportional to transmittance are simultaneously measured.

The description of the detected signals is performed within the Jones matrix formalism [17]. Polarization of the light incident on the sample is described by a combination of 2×2 matrices and a polarization vector of the laser radiation:

$$\mathbf{P}_{in} = \begin{pmatrix} -1 & -1 \\ -1 & 1 \end{pmatrix} \begin{pmatrix} 1 & 0 \\ 0 & e^{i\phi(t)} \end{pmatrix} \times \begin{pmatrix} -1 & -1 \\ -1 & 1 \end{pmatrix} \begin{pmatrix} 1 \\ 0 \end{pmatrix} = \begin{pmatrix} 1 + e^{i\phi(t)} \\ 1 - e^{i\phi(t)} \end{pmatrix}. \quad (2)$$

Here from right to left: the vector for the horizontally polarized light, the first half-wave plate matrix, the PEM matrix, the second half-wave plate matrix. All matrices and vectors are written in the basis of horizontally and vertically polarized waves. Matrices and vectors are written with the normalizing coefficients omitted since they do not affect the observed values. The polarization state of light coming to the detector can be written as follows:

$$\mathbf{P}_{out} = M_{sam}\mathbf{P}_{in} = \begin{pmatrix} ae^{i\varphi} & 0 \\ 0 & b \end{pmatrix} \times \begin{pmatrix} 1 + e^{i\phi(t)} \\ 1 - e^{i\phi(t)} \end{pmatrix} = \begin{pmatrix} ae^{i\varphi}(1 + e^{i\phi(t)}) \\ b(1 - e^{i\phi(t)}) \end{pmatrix}, \quad (3)$$

where M_{sam} is the Jones matrix of the plasmonic nanograting with the nanowires oriented along the horizontally polarized light, a and b are the electromagnetic waves amplitudes measured in the near-field regime for horizontal and vertical incident light polarizations, φ is the sample-induced phase delay between the polarization eigenstates. The intensity of the detected signal within the constant multiplier accuracy is equal to

$$I = a^2 + b^2 + (a^2 - b^2)\cos[A\sin(2\pi ft)]. \quad (4)$$

The right-hand side of the Eq. (4) after the Fourier series decomposition and neglecting the $2\pi f$ harmonics higher than the second one is written as follows:

$$I = a^2 + b^2 + (a^2 - b^2)J_0(A) + 2J_2(A)(a^2 - b^2)\cos(4\pi ft), \quad (5)$$

where $J_0(A)$ and $J_2(A)$ are the Bessel functions of the zeroth and second orders, respectively. The phase delay amplitude for PEM was set to $A = 2.405$ to achieve $J_0(A) = 0$. The signal measured with the lock-in amplifier at the $2f$ frequency is equal to $U_{2f} = 2J_2(A)(a^2 - b^2)$. The signal measured by the ADC after the low-pass filter is $U_{DC} = a^2 + b^2$. Thus the linear dichroism value is expressed in terms of the measured quantities as follows:

$$D_{nf} = \frac{a^2 - b^2}{a^2 + b^2} = \frac{U_{2f}}{2J_2(A)U_{DC}}. \quad (6)$$

A point-by-point evaluation of the map of linear dichroism is performed using Eq. (6) and the maps of U_{2f} and U_{DC}. The calibration of the U_{2f}/U_{DC} ratio is performed by measuring these values with a polarizer with $D \sim 1$ in front of the sample [18]. Then ratio U_{2f}/U_{DC} obtained for the nanowire sample is divided by the value acquired during the calibration.

Figure 3a shows the distribution of D_{nf} in the vicinity of the sample. A periodic array of the well-resolved wires is revealed. The contrast defined as $(D_{nf,\,max} - D_{nf,\,min})/(D_{nf,\,max} + D_{nf,\,min})$ is about 0.3. In addition, peculiarities related to the defects on the sample surface are observed. Figure 3b shows a cross-section of

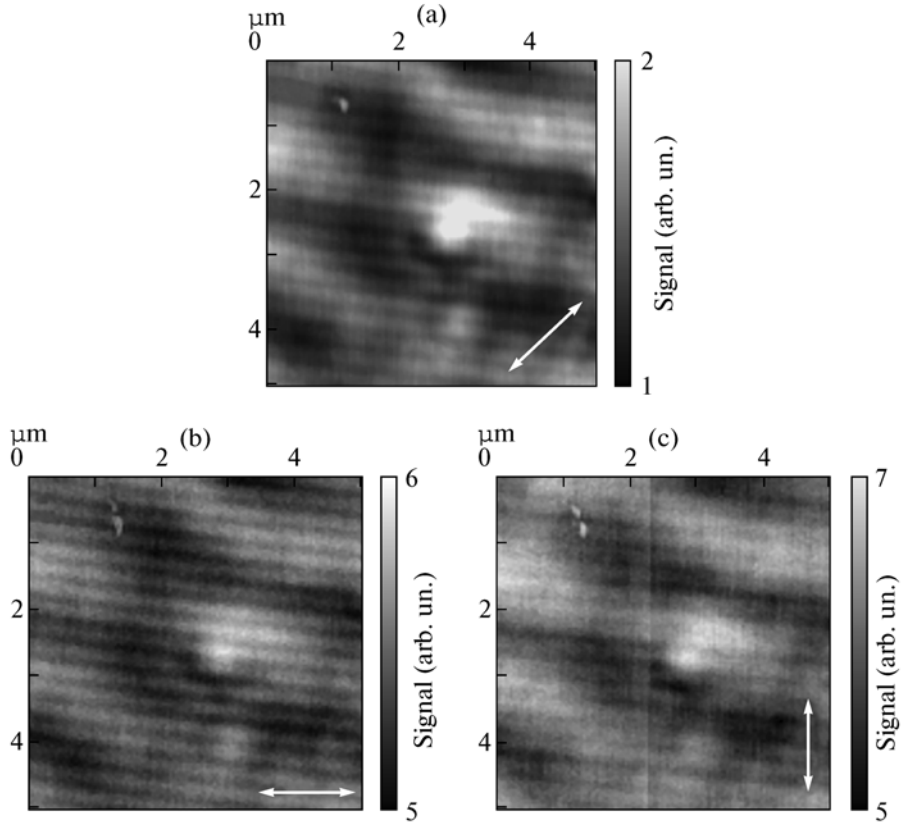

Fig. 4. Scanning near-field optical microscopy images of (a) the nanograting sample obtained without intensity modulation and (b, c) the sample illuminated with intensity-modulated linearly polarized light. The arrows depict the incident light polarization orientation.

the $D_{nf}(x, y)$ map. D_{nf} varies from 0.40 ± 0.05 to 0.75 ± 0.05, the mean value is $D_{nf} \simeq 0.55 \pm 0.05$ which is substantially different from the far-field value $D_{ff}(\lambda = 532\ \text{nm}) \simeq 0.2$. This phenomena can be related both to the sensitivity of the near-field probe to the light polarization and to the linear dichroism increase in the near-field in plasmon-active media. Figure 3c shows the results of the simultaneous measurements of optical and topography signals demonstrating mutual arrangement of the topography peculiarities and the local-field intensity distribution. The local light intensity between the nanowires appears to be higher than beneath them.

The high contrast is achieved in the $D_{nf}(x, y)$ distribution by using the polarization modulation. Figure 4 shows optical images obtained with three different experiment configurations without the polarization modulation for the sample area shown in Fig. 3a. Figure 4a image was obtained with the angle between polarization plane and the nanowires equal to 45°. Figures 4b and 4c show the distribution of the optical signal when intensity modulation was applied to the light linearly polarized along and perpendicular to the nanowires, respectively. It is shown that the speckle peculiarities make the main contribution to the electromagnetic field distribution in Fig. 4 while in Fig. 3a they are considerably fainter. Periodic modulation contrast in Fig. 4b and 4c is 10^{-2} and 5×10^{-3}, respectively, while the speckle contrast is 0.09 and 0.17, respectively. The grating-induced contrast is twice smaller under plasmon-polaritons excitation conditions than in the case the polarization is oriented along the nanowires. This result can be explained by the increase of the effective cross-section of individual nanowire due to the local field enhancement under the resonance of local plasmon-polaritons.

The description of the polarization of electromagnetic radiation by Jones method uses the assumption that the waves are transverse and can be fully described by three parameters, namely amplitudes and relative phase of the waves of orthogonal linear polarizations. However, optical near-fields support non-radiating solutions which are not transverse and for this reason the polarization cannot be defined by three independent parameters. Nevertheless, the linear dichroism formalism can be translated into the optical near-field and formulated as the difference between intensities of SNOM-measured orthogonally polarized field com-

ponents which are localized in the optical near-field of the sample and parallel to the incident orthogonal linearly polarized waves.

To conclude, the effect of linear dichroism is found in the optical near-field of plasmon-active subwavelength nanostructures under the conditions of local plasmon-polariton excitation. The spatial distribution of the linear dichroism value measured with the scanning near-field optical microscopy and dynamic polarimetry methods reveals the contrast of 0.3 at the distance of $\lambda/20$ from the sample surface.

This work was supported by the Russian Foundation of Basic Research, project nos. 10-02-91170 and 10-02-92115, and by Russian Ministry of Education and Science, contract nos. P918, P946, P1465, and 14.740.11.0697.

REFERENCES

1. D. K. Gramotnev and S. I. Bozhevolnyi, Nature Photon. **4**, 83 (2010).
2. S. I. Bozhevolnyi, V. S. Volkov, E. Devaux, et al., Nature Lett. **440**, 508 (2006).
3. J. A. Dionne, K. Diest, L. A. Sweatlock, and H. A. Atwater, Nano Lett. **9**, 897 (2009).
4. D. W. Pohl, W. Denk, and M. Lanz, Appl. Phys. Lett. **44**, 651 (1984).
5. M. Sandtke, R. J. P. Engelen, H. Schoenmaker, et al., Rev. Sci. Instrum. **79**, 013704 (2008).
6. M. Zavelani-Rossi, M. Celebrano, P. Biagioni, et al., Appl. Phys. Lett. **92**, 093119 (2008).
7. C. Durkan and I. V. Shvets, J. Appl. Phys. **83**, 1837 (1998).
8. M. V. Bashevoy, A. A. Ezhov, S. A. Magnitskii, et al., Int. J. Nanosci. **3**, 105 (2004).
9. A. A. Ezhov, S. A. Magnitskii, N. S. Maslova, et al., JETP Lett. **82**, 599 (2005).
10. W. Chen, D. C. Abeysinghe, R. L. Nelson, and Q. Zhan, Nano Lett. **10**, 2075 (2010).
11. G. Schider, J. R. Krenn, W. Gotschy, et al., J. Appl. Phys. **90**, 3825 (2001).
12. M. R. Shcherbakov, P. P. Vabishchevich, M. I. Dobynde, et al., JETP Lett. **90**, 433 (2009)].
13. M. R. Shcherbakov, M. I. Dobynde, T. V. Dolgova, et al., Phys. Rev. B **82**, 193402 (2010).
14. H. C. van de Hulst, *Light Scattering by Small Particles* (Dover, New York, 1981).
15. P. K. Cheo and C. D. Bass, Appl. Phys. Lett. **18**, 565 (1971).
16. D. V. Kazantsev, Instrum. Exp. Tech. **48**, 807 (2005).
17. A. Gerald and J. M. Burch, *Introduction to Matrix Methods in Optics* (Wiley, New York, 1975).
18. A. F. Drake, J. Phys. E: Sci. Instrum. **19**, 170 (1986).